Seismic soil-structure interaction study of inclusion reinforced foundations with a macro-element

Journal of Physics: Conference Series **2647** (2024) 082016 doi:10.1088/1742-6596/2647/8/082016

Seismic soil-structure interaction study of inclusion reinforced foundations with a macro-element

Yuxiang Shen[1,2], Jesús Pérez-Herreros[2], Fahd Cuira[2], Jean-François Semblat[1], Sébastien Burlon[2]

[1] IMSIA (UMR 9219), CNRS, EDF, CEA, ENSTA Paris, Institut Polytechnique de Paris, Palaiseau, France
[2]Terrasol, Setec Group, Paris, France

E-mail: yuxiang.shen@setec.com

Abstract. The reinforcement technique using rigid inclusions is a practical, cost-effective, and time-saving foundation solution. This technique has already proven successful in supporting structures that are subject to high seismic demands, such as the Rio-Antirrio bridge in Greece. In a performance-based design approach, it is important to consider the dynamic soil-structure interaction phenomenon, which is specially relevant when dealing with soft soils. Direct approaches simulating the whole soil-structure system within the same numerical model are still computationally expensive and the classic modal response spectrum analyses, based on the superposition principle, are not capable of taking into account most of nonlinear mechanisms. The macro-element approach is therefore a promising method, as it allows modelling of non-linear soil-structure interaction mechanisms at the base of the structure without increasing the numerical cost. This approach has shown particularly good performance in the dynamic analysis of shallow and piled foundations. The present paper aims to extend the application of the macro-element approach to foundations on rigid inclusions. To this end, the upper-bound kinematic exterior approach is employed to derive a yield surface corresponding to this type of foundation. Its potential application in the context of non-linear soil-structure interaction studies is also discussed.

1. Introduction

The reinforcement technique with rigid inclusions (RIs) is an alternative foundation solution that offers significant technical and economic advantages over the conventional pile foundation design. Over the past twenty years, this technique has been the focus of several research studies, leading to practical recommendations such as those of the ASIRI French National Project [1]. Most of these studies have focused on the static behaviour of rigid inclusion (RI) reinforced foundations, and there has been limited attention to their behaviour under vibratory and seismic loading. Therefore, further research is needed to investigate the dynamic behaviour of RI reinforced foundations, especially under seismic loading conditions.

In earthquake engineering, soil-structure interaction (SSI) is an important phenomenon that must be taken into account to accurately simulate the non-linear behaviour of the soil-foundation-structure system. However, direct approaches simulating the entire soil-structure system within the same numerical model are still computationally expensive. Additionally, classic modal response spectrum analyses, based on the superposition principle, are not capable of taking into account most nonlinear mechanisms. The macro-element approach is therefore

a promising method to model non-linear SSI mechanisms at the base of the structure at low computational cost.

In a macro-element model, the behaviour of the foundation is described by means of a non-linear constitutive law, described in terms of generalized forces (moments) and displacements (rotations) at its centre [2–6]. Most of the available foundation macro-element solutions are formulated within the classical elastoplasticity framework. A yield surface is therefore needed to model the non-linear behaviour and can be derived from the interaction curves in the (V, H, M) space. These curves can be obtained though various methods, such as physical experiments, analytical developments and numerical simulations [7–13].

The present paper aims to extend the application of the macro-element approach to foundations on RIs (in addition to already available solutions for shallow and piled foundations). To this end, the upper-bound kinematic exterior approach is employed by means of an analytical calculation method to determine the bearing capacity of a strip foundation reinforced with RIs. The resulting failure surface can be used in a macro-element for RI reinforced foundations and thus directly applied to non-linear soil-structure interaction analysis.

2. Bearing capacity of a strip footing on homogeneous cohesive and frictional soils

The kinematic exterior approach has been employed in previous work to investigate the bearing capacity of strip footings situated on homogeneous cohesive and frictional soils subjected seismic loading [7, 8, 10, 14, 15]. Various virtual velocity fields have been suggested to determine the stability domain, as shown in Figures 1 and 2.

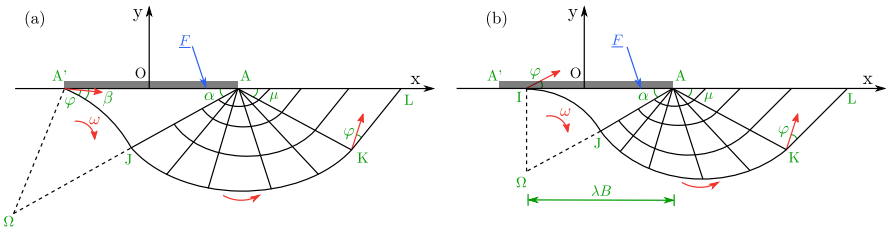

Figure 1. Velocity fields for a rigid strip foundation on frictional soil [10] (a) without uplift, (b) with uplift

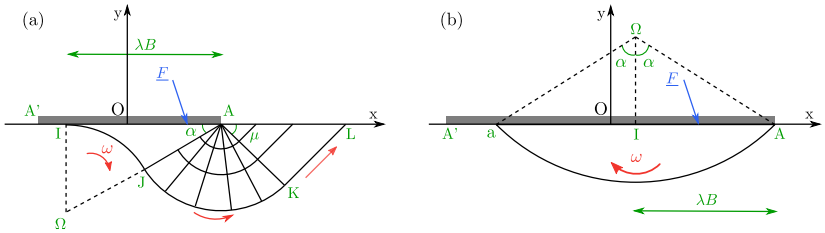

Figure 2. Velocity fields for a rigid strip foundation on coherent soil [14] (a) shear-rotation with uplift, (b) rotation with uplift

3. Upper-bound limit analysis of the bearing capacity of a strip footing on reinforced soil with rigid inclusions

3.1. Problem description

The problem being investigated in this study involved a strip footing subjected to seismic loading. The foundation is placed on a half-space consisting of a load transfer platform (LTP) of thickness h_{LTP} and with a friction angle φ (purely frictional behavior), as well as a cohesive soft soil layer with a cohesion value c and no tensile strength. The soft soil layer is reinforced with RIs, as illustrated in Figure 3.

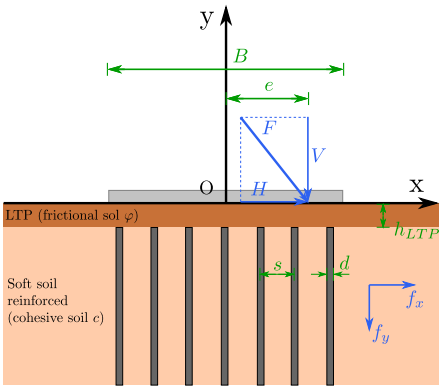

Figure 3. Two-dimensional problem of the bearing capacity of a strip footing reinforced with RIs and subjected to seismic loading

To model the seismic loading on the foundation, the (V, H) couple of forces is considered, representing the inertial forces transmitted by the structure. The force transmitted to the footing is denoted as $\underline{F}$, and the moment $\underline{M}$ is calculated by multiplying the vertical force $\underline{V}$ by the eccentricity e. The inertial effects in the soil are also taken into account by means of body forces due to seismic and gravity loading. They are denoted $f_x = \rho a_h$ and $f_y = \rho g$, respectively. It should be noted that assuming constant inertial forces f_x is acceptable if the failure mechanism is limited to a region near the ground surface. In practice, for shallow failure mechanisms, this assumption is generally valid and does not lead to significant error [14, 16].

3.2. Kinematic exterior approach

The kinematic exterior approach (KEA) is an upper-bound limit analysis method that evaluates kinematically admissible failure mechanisms $\underline{\widehat{U}}$ and checks whether the virtual power of external loads applied to the system P_e is less than or equal to the maximum resistant power of the soil P_{rm}. An upper-bound K is included in the space defined by the inequation (1) [17].

$$K \subset \{P_{rm}(\underline{\widehat{U}}) \geq P_e(\underline{\widehat{U}})\} \tag{1}$$

The maximum resistant power P_{rm} is equal to:

$$P_{rm} = \int_{\Omega} \pi(\underline{\widehat{d}}) d\Omega + \int_{\Sigma} \pi(\|\underline{\widehat{U}}\|) d\Sigma \tag{2}$$

Where π denotes the density of the virtual power in function of the strain rate $\underline{\widehat{d}}$ of the volume Ω and the virtual velocity $\|\underline{\widehat{U}}\|$ at the discontinuity surface Σ.

For a material without tensile strength [17]:

- In the volume:

$$\pi(\underline{\widehat{d}}) = \begin{cases} +\infty & \text{if} \quad tr(\underline{\widehat{d}}) < 0 \\ C[|\widehat{d}_1| + |\widehat{d}_2| + |\widehat{d}_3|] & \text{if} \quad tr(\underline{\widehat{d}}) \geq 0 \end{cases} \tag{3}$$

- Along the lines of velocity discontinuity, with normal vector $\underline{n}$:

$$\pi(\|\underline{\widehat{U}}\|) = \begin{cases} +\infty & \text{if} \quad \|\underline{\widehat{U}}\| \cdot \underline{n} < 0 \\ C[\|\underline{\widehat{U}}\| - \|\underline{\widehat{U}}\| \cdot \underline{n}] & \text{if} \quad \|\underline{\widehat{U}}\| \cdot \underline{n} \geq 0 \end{cases} \tag{4}$$

The virtual power of all the external forces applied to the system P_e includes the loads applied on the foundation $\underline{F}$ (V, H, M) and the body forces (f_x, f_y) generated by inertia in the soil.

In the case of a foundation reinforced with RIs, the expression of P_e remains unchanged compared to the case without reinforcement (see §2). However, the expression of P_{rm} needs to consider the contribution of RI reinforcement, denoted P_{RI} (see §3.3).

In order to validate the calculation code used in this study, the first step was to study the failure mechanisms described in the literature for a strip footing on homogeneous cohesive and frictional soils and to compare the results (see Figures 4, 5,6 and 7).

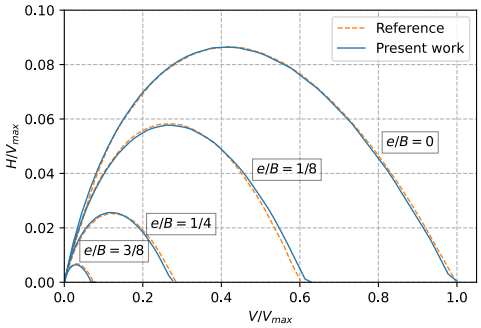

Figure 4. Interaction curves $H-V$ under eccentric load for a strip foundation on frictional soil, compared with ref. [10]

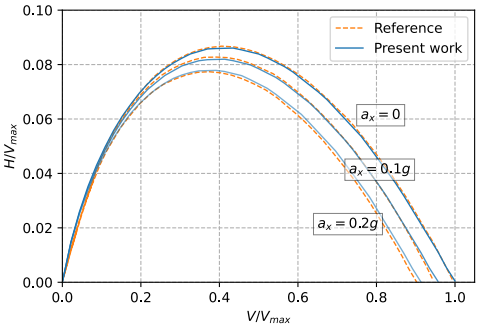

Figure 5. Interaction curves $H-V$ with soil inertia for a strip foundation on frictional soil, compared with ref. [10]

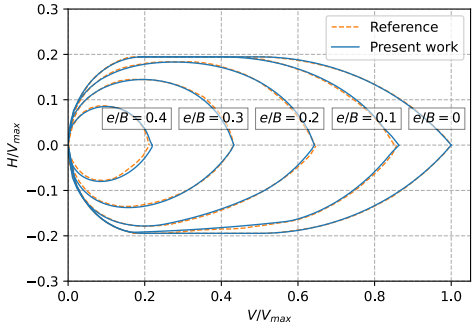

Figure 6. Interaction curves $H-V$ under eccentric load for a strip foundation on cohesive soil, compared with ref. [8]

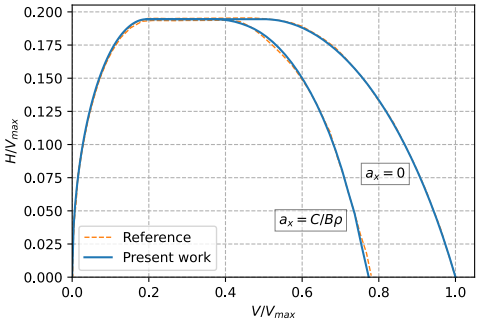

Figure 7. Interaction curves $H-V$ with soil inertia for a strip foundation on cohesive soil, compared with ref. [9]

3.3. Failure analysis of rigid inclusions

The inclusions are taken into account by considering their action at the intersection with the rupture surface. The forces at the intersection are decomposed into an axial force T_n, a shear force T_c and a bending moment M_c. However, these forces are limited by several criteria :

(i) Material intrinsic strength
(ii) Vertical soil-inclusion interaction resistance
(iii) Lateral soil-inclusion interaction resistance: plastification of the soil
(iv) Lateral soil-inclusion interaction resistance: plastification of the inclusion

3.3.1. Material intrinsic strength

This criterion corresponds to the failure of the inclusion by breakage [18]. The combination of T_n, T_c and M_c that occurs at the intersection of the inclusions and the velocity discontinuity

surface can be represented by the following simple expression (see Equation (5)), proposed by Anthoine [19].

$$\left(\frac{T_n}{V_0}\right)^2 + \left(\frac{T_c}{H_0}\right)^2 + \left|\frac{M_c}{M_0}\right| \leq 1 \tag{5}$$

Where V_0, H_0, M_0 are the limits of the material intrinsic strength. The form of this criterion is an ellipse in the (T_n, T_c) plan. The same expression has also been used in the study of nail reinforced slopes to evaluate the material inherent resistance [18, 20, 21].

3.3.2. Axial soil-inclusion interaction limit
The maximal axial force which can be provided by RIs are controlled by the lateral friction and the forces at the head and tip of the inclusion by an internal "pullout" failure (see Equation (6)).

$$T_{nl} = min(F_{head} + q_s l_{int} \pi d, F_{tip} + q_s l_{ext} \pi d) \tag{6}$$

3.3.3. Lateral soil-inclusion interaction limit
This criterion corresponds to the limit of the lateral soil-inclusion interactive behaviour. The pressure of the interior part (L_{int}) or the exterior part (L_{ext}) of the inclusion is limited by the limit pressure in the soil p_l^*. The lateral pressure distributions for different lengths of L_{int} and L_{ext} are illustrated in Figure 8.

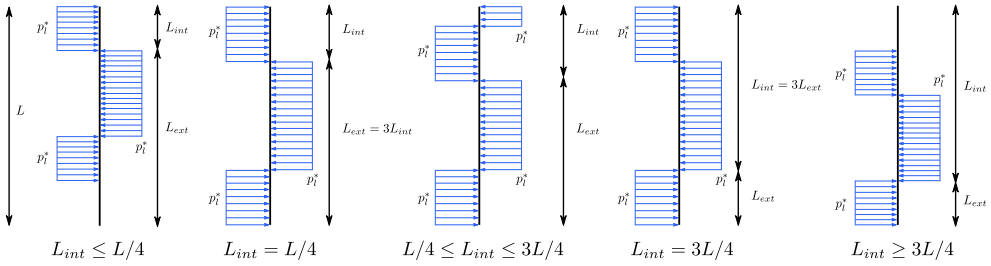

Figure 8. Lateral pressure transmitted to the soil along the inclusion length by means of a limit analysis approach

The inclusions may also fail at the location where the maximum bending moment is found. In this case, the shear force is zero, and the expression in Equation (5) can be simplified to Equation (7). Figure 9 shows the normalised values of T_c, M_c and M_{max} for different values of L_{int}/L.

$$M_{max} \leq M_0[1 - (\frac{T_n}{V_0})^2] \tag{7}$$

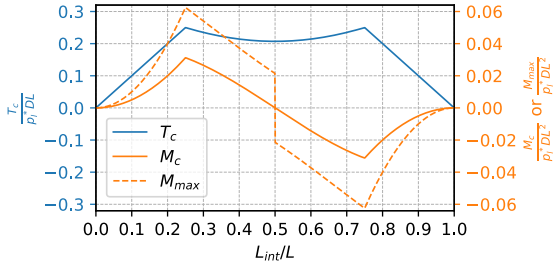

Figure 9. T_c, M_c and M_{max} for different L_{int}/L values

3.3.4. Multicriterion of Rigid Inclusion failure mode
The combination of the four criteria mentioned above in the (T_n, T_c) plane defines a useful stability domain, called multicriterion [18], which limits the development of axial and shear forces (T_n, T_c). This stability domain can be visualised as an envelope of the four criteria. The forces in the inclusion can be placed at any point within the useful domain (see Figure 10). However, when failure occurs, the point (T_n, T_c) should be at the boundary of the useful domain, and its position is determined by the rule of maximum work [22]. This means that the position of the point (T_n, T_c) on the boundary is chosen to maximise the work of the inclusion in a considered failure mechanism. Once the virtual velocity at the intersection of the inclusion with the failure surface is given, the virtual power of the inclusion can be calculated.

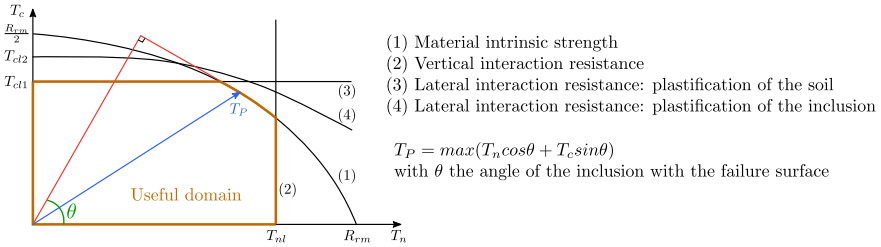

Figure 10. Multicriterion combining several failure criteria in (T_n, T_c) plane [18]

3.4. Multicriterion upper-bound limit analysis combining multiple simplified sub-systems
Compared to the previous cases where the footing rests directly on an infinite homogeneous half-space, the case of a footing on a soil reinforced with RIs is characterised by the presence of a LTP between the foundation and the reinforced soil. Therefore, the reinforcement and the bi-layer configuration differ the failure mechanisms for RI reinforced foundation from those for foundation without reinforcement.

To account for these peculiarities, the three simplified sub-systems (see Figure 11) were studied by means of an upper-bound limit analysis and their results were superimposed to determine the bearing capacity of a foundation on RIs:

- Case I: Homogeneous frictional soil without reinforcement for failure concentrated in the LTP (the depth of the failure mechanism is thus lower than h_{LTP}).
- Case II: Sliding and uplift at the interface between the LTP and the reinforced soft soil.
- Case III: Homogeneous cohesive soil considering reinforcement with RIs (the depth of the failure is greater than h_{LTP} and intersects the RIs).

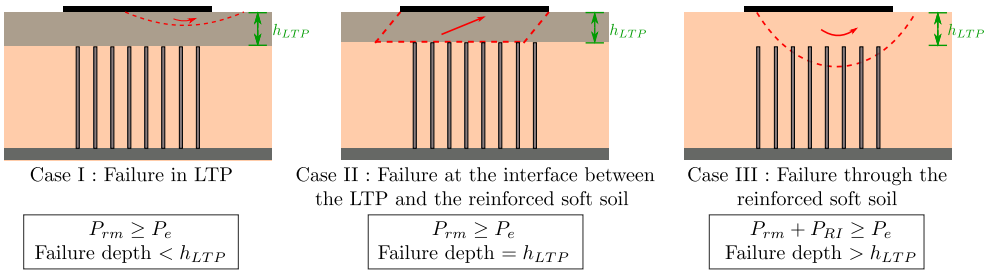

Figure 11. Simplified cases for upper-bound limit analysis

Case I is particularly relevant to consider the failure mechanisms in the LTP, which are expected to replicate the same failure mechanisms considered for the failure of shallow foundations on frictional soil (see Figure 1). Case III, on the other hand, focuses on the potential failure modes occurring in the reinforced soft soil with RIs. The same failure modes as for cohesive soil are considered (see Figure 2). Case II is added in order to simulate a transition mode between the shallow failure mechanisms (Case I) and the deep failure mechanisms (Case III). This failure mechanism is inspired by the F_0 mechanism presented in reference [8].

3.5. Case study

3.5.1. Studied configuration

In this study, a typical foundation configuration with rigid inclusion reinforcement was considered. It consists of a 10 m wide strip footing, resting on a 0.5 m thick LTP with a friction angle of 38°. The soft soil, considered to be cohesive, has a cohesion of 25 kPa ($q_s = 25$ kPa and $p_l = 200$ kPa). Concrete RIs, 0.4 m in diameter and 10 m long, are present throughout the depth of the soft soil, without penetrating the LTP. A axis-to-axis spacing of 1.5 m is considered, resulting in a substitution rate of 5.6 %.

3.5.2. Determination of an upper-bound of the limit load

The interaction curves in the $V - H$ plane were calculated for the three simplified cases (see §3.4) and then superimposed, as shown in Figure 12. The result of the superimposition revealed that the $V - H$ interaction curve is composed of three parts. The left part is controlled by case I, which represents failure in the LTP. The right part is controlled by case III, which represents failure in the reinforced soft soil. These two curves are limited by case II, which represents failure at the interface of the LTP and soft soil.

The results showed that the RIs in the foundation system can significantly increase its ultimate bearing capacity under centred vertical loading. Specifically, the ultimate bearing capacity increased by approximately 1.8 times, from 1285 kN to 2266 kN, when compared to the same strip footing on soft soil without reinforcement. It is interesting to note that the maximum admissible horizontal force was not improved with the presence of RIs and remained the same as the non-reinforced strip foundation.

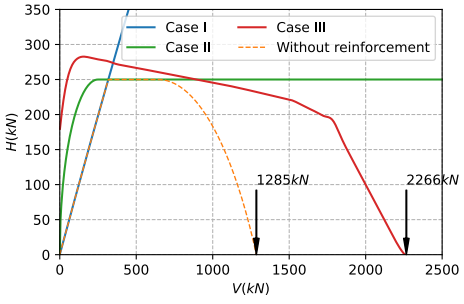

Figure 12. Superimposition of the interaction curves of the three simplified sub-systems

3.5.3. Load eccentricity effects

The $V - H$ interaction diagrams for various load eccentricities ($e = M/V$) are presented in Figure 13. It can be observed that as the load eccentricity increases, both the ultimate bearing capacity and the maximum horizontal forces decrease.

Figure 14 presents the bearing capacities $V_{max,e}$ for both the reinforced and non-reinforced foundations under different load eccentricities e, normalised by those without eccentricity $V_{max,e=0}$. In addition, the result were compared with the conventional eccentricity correction factor i_e proposed by Meyerhof [23].

It can be observed that the proposed i_e is more conservative than the value obtained by upper-bound limit analyses. However, it is evident that the impact of load eccentricity is more significant for the foundation reinforced with RIs than for the non-reinforced one. For an eccentricity $e/B = 0.2$, the strip foundation can still retain 64% of the ultimate bearing capacity, while the RI reinforced foundation can only support 53% of the ultimate bearing capacity. Nonetheless, it is crucial to note that the ultimate bearing capacity of the reinforced foundation always exceeds that of the non-reinforced foundation, even when subjected to a load with an eccentricity of $e/B = 0.2$.

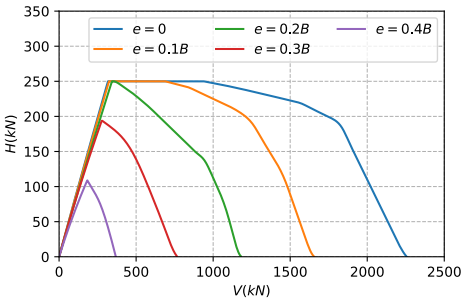

Figure 13. $V - H$ interaction curves for different load eccentricities

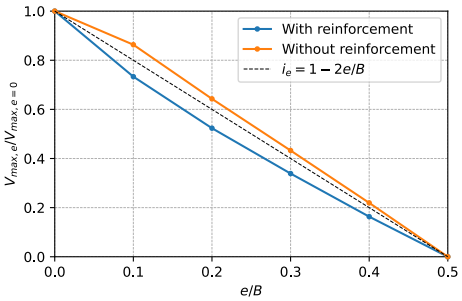

Figure 14. Ultimate bearing capacity reduction for different load eccentricities

3.5.4. Soil inertia effects

Soil inertia effects were also analysed in the present study. Figure 15 displays the $V - H$ interaction curves for several maximum acceleration values in the soil ranging from 0 to $0.5g$. It is observed that the shape of the $V - H$ interaction curves is not affected by the soil inertia effects and that only the amplitude of their right-hand side, controlled by case III, is impacted by soil inertia.

Figure 16 investigated the reduction of the ultimate bearing capacity due to soil inertia. It is shown that the RI improvement increases the foundation's capacity to carry soil inertia. For example, for a critical soil inertia force $\bar{F}_{cr} = 1.5$ (i.e., corresponding to $a_h = 0.1875g$, $\rho = 2\ t/m^3$, $B = 10\ m$ and $c = 25\ kPa$), the non-improved foundation loses half of its ultimate bearing capacity due to soil inertia effects. In contrast, the inclusion reinforced strip foundation can still retain up to 85% of its ultimate bearing capacity. Furthermore, it can be found that once the critical soil inertial force $\bar{F}_{cr}$ reaches 1.6, the non-reinforced foundation is unable to maintain equilibrium with any external forces at the footing. On the other hand, with RI reinforcement, the critical soil inertia force $\bar{F}_{cr}$ can reach up to 4, while the ultimate bearing capacity is reduced by only 58%.

4. Macro-element model for a foundation reinforced with rigid inclusions

4.1. Elastic response

Under low to moderate amplitude loads, a RI reinforced foundation exhibits an elastic response. Recent studies [24, 25] have focused on the dynamic impedances of shallow foundations on reinforced soils using a substructuring approach and an equivalent linear approximation to model the soil behaviour. An important conclusion of these studies is that the coupling terms in the dynamic impedance matrix are negligible, i.e. the elastic response of these foundations can be modelled by independent linear springs for each degree of freedom. For a macro-element not taking into account the torsional moment M_z, the following stiffness matrix is considered at the base of the structure.

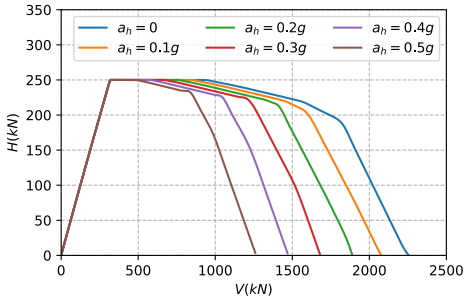

Figure 15. $V - H$ interaction curves for different soil inertiae

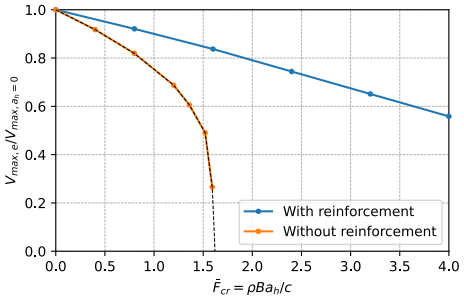

Figure 16. Ultimate bearing capacity reduction for different soil inertiae

$$\underline{\underline{F}} = \begin{bmatrix} H_x \\ H_y \\ V \\ M_{rx} \\ M_{ry} \end{bmatrix} \qquad \underline{\underline{K}}^{el} = \begin{bmatrix} K_{xx} & & & & \\ & K_{yy} & & & \\ & & K_{zz} & & \\ & & & K_{rx} & \\ & & & & K_{ry} \end{bmatrix} \tag{8}$$

4.2. Plastic response

The plastic mechanism can be simulated using a yield surface and an appropriate plastic flow rule. The yield surface for a foundation reinforced with RIs can be obtained through the upper-bound limit analysis with an associated plastic flow rule. A generalized expression such as the one in Equation (9) [26] can be fitted to reproduce as close as possible the multicriterion upper-bound stability domain resulting from the application of §3.4.

$$f(V, H, M) = \left(\frac{H}{aV^c(1-V)^d}\right)^2 + \left(\frac{M}{bV^e(1-V)^f}\right)^2 - 1 = 0 \tag{9}$$

The addition of a relevant hardening law into the macro-element can improve its ability to reproduce a cyclic behaviour under seismic loading, if necessary.

5. Conclusions

A brief review of the failure mechanisms of a strip foundation on homogeneous frictional and cohesive soil already available in the literature was first performed. The results of these studies and several of the proposed virtual velocity fields were then adapted to the study of the bearing capacity of a strip foundation on a soil reinforced with rigid inclusions.

A multi-step approach based on the theory of limit analysis (a kinematic exterior approach) was introduced to determine the yield surface for this type of foundations. Due to the complexity of reinforced strip foundation configurations, a set of simplified sub-systems were first studied separately and then combined into a final interaction curve delimiting the stability domain.

A case study allowed to confirm that the presence of RIs increases the ultimate bearing capacity. Different load eccentricity and soil inertia values were studied. It was observed that the reinforced configuration is more affected by load eccentricity than the same foundation on a non-reinforced soil, with a more significant reduction in ultimate bearing capacity due to load eccentricity than the conventional reduction factor i_e. The parametric study conducted for several values of peak ground acceleration confirmed that RIs can significantly reduce the impact of soil inertia due to seismic motion. This finding confirmed the interest of using RI reinforced foundations in high seismic hazard zones.

Finally, the necessary adaptations in a macro-element approach to model the elastic and plastic response of the foundation were identified. The interest and potential of using the results from the limit analysis of the foundation to develop a SSI macro-element for engineering applications was demonstrated.

References

[1] ASIRI 2012 *Recommandations pour la conception, le calcul, l'exécution et le contrôle des ouvrages sur sols améliorés par inclusions rigides verticales* (Presses des Ponts)
[2] Paolucci R, Shirato M and Tolga Yilmaz M 2008 Seismic behaviour of shallow foundations: Shaking table experiments vs numerical modelling *Earthquake Eng. Struct. Dyn.* **37** 577–95
[3] Grange S, Kotronis P and Mazars J 2008 A macro-element for a shallow foundation to simulate Soil-Structure Interaction considering uplift *C.R. Mec.* **336** 856–62
[4] Chatzigogos C T, Pecker A and Salençon J 2009 Macroelement modeling of shallow foundations *Soil Dyn. Earthquake Eng.* **29** 765–81
[5] Abboud Y 2017 *Développement d'un macroélément pour l'étude des fondations superficielles sous charge sismique* Ph.D. thesis Université Paris-Est
[6] Pérez-Herreros J 2020 *Dynamic soil-structure interaction of pile foundations : experimental and numerical study* Ph.D. thesis Ecole Centrale Nantes
[7] Salençon J and Pecker A 1995 Ultimate bearing capacity of shallow foundations under inclined and eccentric loads. Part I: purely cohesive soil *Eur. J. Mech. A. Solid* **14** 349–75
[8] Salençon J and Pecker A 1995 Ultimate bearing capacity of shallow foundations under inclined and eccentric loads. part II: purely cohesive soil without tensile strength *Eur. J. Mech. A. Solid* **14** 377–96
[9] Pecker A 1997 Analytical formulae for the seismic bearing capacity of shallow strip foundations *Seismic Behaviour of Ground and Geotechnical Structures* (CRC Press) pp 261–68
[10] Paolucci R and Pecker A 1997 Seismic bearing capacity of shallow strip foundations on dry soils *Soils Found.* **37** 95–105
[11] Soubra A H 1999 Upper-Bound Solutions for Bearing Capacity of Foundations *J. Geotech. Geoenviron. Eng.* **125** 59–68
[12] Chatzigogos C T, Pecker A and Salençon J 2005 Seismic bearing capacity of shallow foundations *11th WCEE* (Acapulco, Mexico)
[13] Li S, Yu J, Huang M and Leung C F 2021 Upper bound analysis of rectangular surface footings on clay with linearly increasing strength *Comput. Geotech.* **129** 103896
[14] Pecker A and Salencon J 1991 Détermination de la capacité portante des fondations superficielles sous sollicitations dynamiques Tech. rep. MRES
[15] Paolucci R and Pecker A 1997 Soil inertia effects on the bearing capacity of rectangular foundations on cohesive soils *Eng. Struct.* **19** 637–43
[16] Chatzigogos C T 2007 *Comportement sismique des fondations superficielles : vers la prise en compte d'un critère de performance dans la conception* Ph.D. thesis École Polytechnique
[17] Salençon J 1983 *Calcul à la rupture et analyse limite* (Paris, France: Presses de l'ENPC)
[18] Schlosser, F and Unterreiner P 1990 Soil Nailing in France: Research and Practice. *Transp. Res. Rec.* **1330** 72–7
[19] Anthoine A 1987 Stabilité d'une fouille renforcée par clouage *4th Franco-Polish Conf. on Appl. of Soil Mech.* (Grenoble, France)
[20] De Buhan P, Dormieux L and Salencon J 1992 An Interactive Computer Software for the Yield Design of Reinforced Soil Structures *Actes du colloque organisé par l'ENPC* (Paris, France)
[21] de Buhan P 2004 Renforcement par inclusions des sols et des roches *Revue Française de Génie Civil* **8** 1033–69
[22] Schlosser F 1978 Behaviour and Design of Soil Nailing *Symp. for Recent Dev. in Ground Improv. Tech.* (Bangkok, Thailand) pp 399–413
[23] Meyerhof G G 1953 The bearing capacity of foundations under eccentric and inclined loads *3rd ICSMFE* (Zurich, Swiss) pp 440–5
[24] Shen Y, Pérez-Herreros J, Cuira F, Semblat J F and Burlon S 2021 Dynamic response of shallow foundations on reinforced soil with rigid inclusions *17th WCEE* (Sendai, Japan)
[25] Shen Y, Pérez-Herreros J, Cuira F, Semblat J F and Burlon S 2022 Interaction inertielle sol-structure d'un massif renforcé par inclusions rigides *11th JNGG* (Lyon, France)
[26] Grange S, Kotronis P and Mazars J 2009 A macro-element to simulate 3D soil-structure interaction considering plasticity and uplift *Int. J. Solids Struct.* **46** 3651–63